Biochemical and Biophysical Research Communications 449 (2014) 107–113

Contents lists available at ScienceDirect

Biochemical and Biophysical Research Communications

journal homepage: www.elsevier.com/locate/ybbrc

Crystal structure studies of NADP$^+$ dependent isocitrate dehydrogenase from *Thermus thermophilus* exhibiting a novel terminal domain

S.M. Kumar [a], K.J. Pampa [b], M. Manjula [a], M.M.M. Abdoh [c], Naoki Kunishima [d], N.K. Lokanath [a,*]

[a] Department of Studies in Physics, University of Mysore, Mysore 570 006, India
[b] Department of Studies in Microbiology, University of Mysore, Mysore 570 006, India
[c] Department of Physics, Faculty of Science, An-Najah National University, Nablus, West Bank, Palestine
[d] Advanced Protein Crystallography Research Group, RIKEN SPring-8 Center, Harima Institute, Hyogo 679-5148, Japan

ARTICLE INFO

Article history:
Received 24 April 2014
Available online 14 May 2014

Keywords:
NADP$^+$ binding loop
Citrate
Unique terminal domain
Oligomerization
Metal ion

ABSTRACT

NADP$^+$ dependent isocitrate dehydrogenase (IDH) is an enzyme catalyzing oxidative decarboxylation of isocitrate into oxalosuccinate (intermediate) and finally the product α-ketoglutarate. The crystal structure of *Thermus thermophilus* isocitrate dehydrogenase (*Tt*IDH) ternary complex with citrate and cofactor NADP$^+$ was determined using X-ray diffraction method to a resolution of 1.80 Å. The overall fold of this protein was resolved into large domain, small domain and a clasp domain. The monomeric structure reveals a novel terminal domain involved in dimerization, very unique and novel domain when compared to other IDH's. And, small domain and clasp domain showing significant differences when compared to other IDH's of the same sub-family. The structure of *Tt*IDH reveals the absence of helix at the clasp domain, which is mainly involved in oligomerization in other IDH's. Also, helices/beta sheets are absent in the small domain, when compared to other IDH's of the same sub family. The overall *Tt*IDH structure exhibits closed conformation with catalytic triad residues, Tyr144-Asp248-Lys191 are conserved. Oligomerization of the protein is quantized using interface area and subunit–subunit interactions between protomers. Overall, the *Tt*IDH structure with novel terminal domain may be categorized as a first structure of subfamily of type IV.

1. Introduction

In the tricarboxylic acid (TCA) cycle, an enzyme isocitrate dehydrogenase [IDH; EC: 1.1.1.42] catalyzes oxidative decarboxylation of substrate (isocitrate) using cofactor (NADP$^+$) and bivalent-metal ion (Mg^{2+} or Mn^{2+}) to form α-ketoglutarate (αKG), CO_2 and NADPH [1–3]. One of the key reactions of TCA cycle is to provide majority of energy to the aerobic organisms and NADP$^+$ dependent IDH's involved in the role of providing glucose to the starving aerobic bacteria dependent on the glyoxylate bypass. This enzyme belongs to the β-decarboxylating dehydrogenase family of bifunctional enzymes that plays explicit roles in energy metabolism, amino acid synthesis and vitamin production [4,5]. Generally, these enzymes are found in archaea, bacteria and eukarya [6]. The IDH also acts as substrate to the kinase phosphate *AceK* hosted in *Escherichia coli* [7–10]. In humans, the IDH performs important actions in cytoplasm and mitochondria. And, their mutation can lead to different types of cancer [11,12]. Recently, the biochemical and structural studies of *Mycobacterium tuberculosois* IDH has allowed to propose a chemical mechanism of IDH [13]. The oxidative damage due to tumor cells can be shielded by mitochondrial NADP$^+$ dependent IDH, which supplies NADPH for antioxidant systems and overall tumorigenesis is suppressed in mice deficient in IDH2 [14]. The characterization of NADP-dependent IDH from *Microcystis aeruginosa* may provide platform for controlling the blue-green algae through the biological techniques [15].

IDH's structures are well studied enzymes with more than 40 structures available in the Protein Data Bank (PDB). Also, they are classified into sub-families of subfamily I (type I), subfamily II (type II) and subfamily III (type III) depending upon the binding of cofactors (NAD$^+$ or NADP$^+$) and their oligomerization form (monomer or dimer) [16]. Archaeal and majority of the bacterial IDH's are grouped under subfamily I, eukaryotic homodimeric IDH's and few bacterial IDH's are categorized as subfamily II, eukaryotic hetero oligomeric IDH's constitute subfamily III. Recently, the bioinformatic studies related to phylogenic study of NADP-IDH's revealed the existence of subfamily IV (type IV) consists of homodimeric *Tt*IDH, having an extended C-terminal region. This extended motif is believed to participate in the oligomerization and signaling [17].

* Corresponding author. Fax: +91 821 2419333.
E-mail address: lokanath@physics.uni-mysore.ac.in (N.K. Lokanath).

http://dx.doi.org/10.1016/j.bbrc.2014.04.164
0006-291X/

Here we present the crystal structure of *Tt*IDH using X-ray diffraction method to a resolution of 1.80 Å. To our knowledge, this is the first IDH crystal structure having unique domain at the C-terminal, which is involved in the oligomerization. The *Tt*IDH structure is compared with homologous IDH structures from *E. coli* (*Ec*IDH:PDB-4AJ3) [18–19], *Bacillus subtilis* (*Bs*IDH), [20] and *Aeropyrum pernix* (*Ap*IDH) [21].

2. Materials and methods

2.1. Protein expression and purification

The protein expression and purification of *Tt*IDH are described qualitatively in the Supplemental document; the purified *Tt*IDH was concentrated to 20.0 mg ml^{-1} by ultrafiltration and was stored at 203 K.

2.2. Crystallization

Crystals of *Tt*PGDH were obtained by the microbatch method using NUNC™ HLA plates (Nalge Nunc International) and the quantitative description is provided in Supplemental document.

2.3. Data collection, processing and structure determination

All X-ray diffraction data sets were collected at the synchrotron beam line BL26B1 at SPring-8, Japan, under cryogenic conditions. In-detail description is available in the supplemental document. Multiwavelength anamolous dispersion [22] data sets were collected to solve the crystal structure of *Tt*IDH. The data were indexed, scaled and prepared using HKL package [23] and CCP4 suite [24]. Data collection parameters and processing statistics are given in Table 1.

2.4. Crystallographic refinement, density modification and model building

SOLVE/RESOLVE [25] was used for phasing and coordinates are refined using CNS [26]. Clear electron density was observed for the cofactor or citrate was bound to the enzyme. The topology and parameter files of the NADP$^+$, and citrate molecules were obtained from the Hetero-compound Information Center of Uppsala on the Uppsala website [27]. Stereochemical quality of the model was checked with the program PROCHECK [28]. The refinement statistics are summarized in Table 1. The final atomic coordinates have been deposited in the RCSB Protein Data Bank (www.rcsb.org/pdb) with the accession codes 2D1C. Complete discussions are available in the Supplemental document.

Table 1
Crystal data, data collection and refinement statistics.

Data statistics	
Space group	$P\,2_1$
Unit-cell parameters (Å, °)	a = 73.02, b = 95.18, c = 72.99; β = 92.07
V_M (Å^3 Da^{-1})	2.3
Content of the asymmetric unit	Dimer
Resolution (Å)	50.0–1.8 (1.86–1.80)
Reflections (measured/unique)	92,458/92,029
R_{merge} (%)	6.1
Completeness (%)	99.8 (99.7)
$\langle I/\sigma(I)\rangle$	9.5 (13.7)
Redundancy	3.3
Refinement statistics	
Resolution (Å)	36.49–1.80
R_{cryst} (%)	20.7
R_{free} (%)	23.8
rms bond lengths (Å)	0.006
rms bond angles (°)	1.3
Ramachandran plot (%)	
Most favored	94.73
Additional	4.46
Generous	0.8

Values in parentheses are for the highest resolution shell.

2.5. Model analysis

DALI [29] (ekhinda.biocenter.helsinki.fi/dali_server/start) server was utilized for structural similarity search against all known structures deposited in the PDB. Figures preparation and superimposition of protein models were performed using PyMol (www.pymol.org). Surface areas for dimer and hydrogen bonds were calculated using PISA [30]. The ionic bridges are calculated using ESRBI [31]. Aromatic–aromatic interactions and cation–pi interactions were calculated using PIC [32]. Multiple sequence alignment is performed using CLUSTALW [33] and the figure is generated using ESPript [34].

3. Results and discussion

3.1. Overall structure of TtIDH

The ternary complex (NADP$^+$ and citrate) structure of *Tt*IDH was determined at 1.80 Å resolution. The Matthew's coefficient (V_M) is 2.30 Å^3/Da and the estimated solvent content is 46.80% [35]. The overall structure of the monomer is as shown in Fig. 1. It consists of mainly three domains large domain, small domain and clasp domain. The large domain consists of N-terminus followed by α + β conformation with residues 1–110 and 259–354. These are assembled to secondary structures β1-β2-β3-α1-β4-β5-α2 and β13-β14-α9-α10-α11-α12, respectively. Small domain shows α/β conformation with residues 111–140 and 165–258 assembled to secondary structures β6-β7 and α5-β10-α6-β11-α7-β12-α8, respectively. The clasp domain consists of residues 141–164 organized to secondary structures β8-turn-β9. In addition, a unique domain is observed at the C-terminal domain from 355 to 496 (approximately 141 amino acids) residues composed of a long loop followed by secondary structures β15-α13-β16-β17-β18-α14-β19-β20. There is no related structure with DALI [29] search that contains novel C-terminal domain structure (cut off *Z*-score is 7).

The overall structure of *Tt*IDH is similar to the *Ec*IDH, *Bs*IDH and *Ap*IDH enzyme; with majority of the secondary structures involved in the catalysis are conserved (Supplemental Fig. S1 and Fig. 2). The region which shows significant differences is in the small and clasp domains. *Tt*IDH donot consists of helices between β8 and β9 in clasp region (red arrow in Fig. 2), which plays a major role in the dimerization and present in all other IDH's of the same family. In the absence of these helices, *Tt*IDH oligomerizes with the novel domain present at the C-terminus protruding to the clasp region and involving in dimerization (red elliptical dotted lines in Fig. 2). This oligomerization is very unique, which is absent in all IDH's.

The small domain region (between α6 and β10; blue arrow; Fig. 2) of *Tt*IDH structure shows a difference when compared to other IDH's. The *Bs*IDH shows an extra insert of two alpha (αg2 and αg3) helices and one beta strand (L) in the same region. In *Ap*IDH, beta strand (L) followed by alpha helix (αg2) is observed. Where, the *Ec*IDH has no alpha helices, instead an additional beta strands (βK and βL) are observed. The phosphorylation loop is indicated by red arrow (Fig. 2) and is conserved among the IDH's.

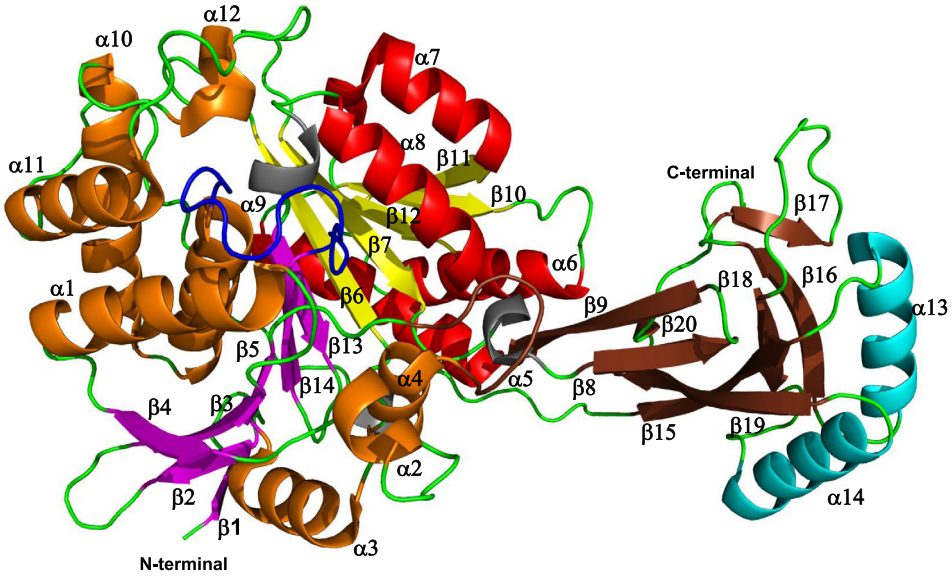

Fig. 1. Overall monomeric structure of *Tt*IDH is resolved into large domain (orange helices and magenta sheets), small domain (red helices and yellow sheets) and clasp domain (cyan helices and chocolate sheets). C-terminus marked with C and N-terminus marked with N. The folds β1-β2-β3-α1-β4-β5-α2 and β13-β14-α9-α10-α11-α12 represents the large domain. Small domain is represented by β6-turn-β7and α5-β10-α6-β11-α7-β12-α8. The clasp domain consists of β8-β9 fold and β15-α13-β16-β17-β18-α14-β19-β20 fold protruding into clasp domain terminated by C-terminal. Blue loop represents the $NADP^+$ binding loop. Brown loop represents the phosphorylation loop. (For interpretation of the references to color in this figure legend, the reader is referred to the web version of this article.)

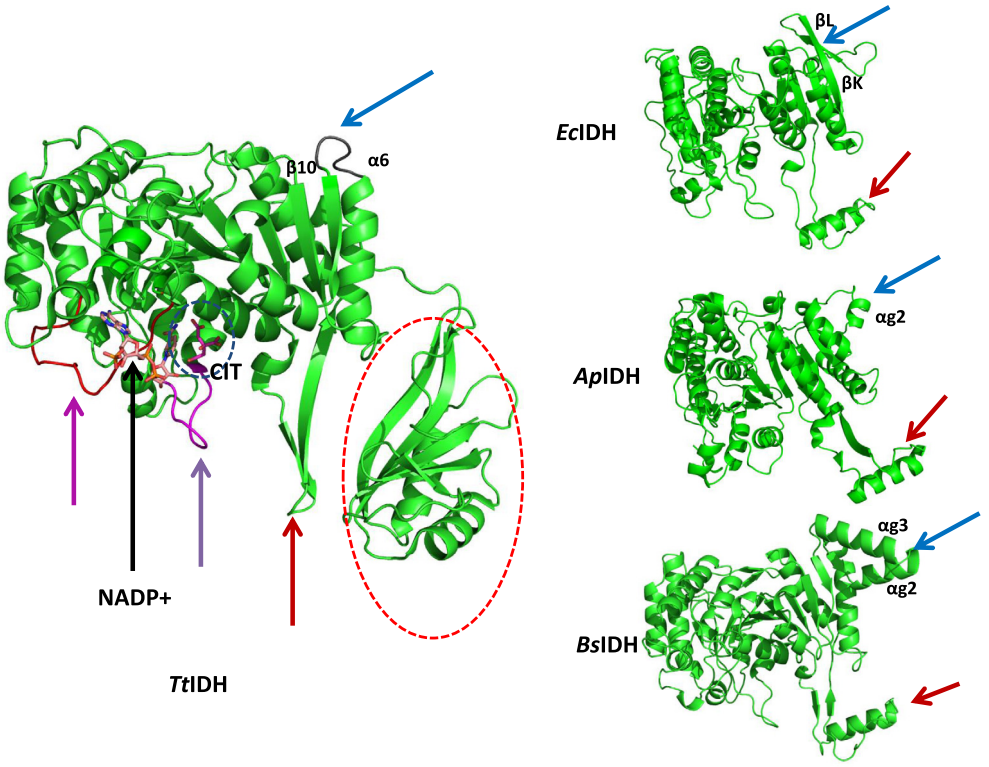

Fig. 2. Monomer comparison (ribbon representation) of *Tt*IDH, *Bs*IDH, *Ec*IDH and *Ap*IDH. Pink arrow in *Tt*IDH represents the $NADP^+$ binding loop (red), Citrate (CIT, magenta stick model-blue dashed line) and $NADP^+$ are represented by ball and stick representation. Purple arrow represents the phosphorylation loop (magenta). Red arrow represents the clasp domain region involved in the oligomerization. Blue arrow (pointed towards grey loop of *Tt*IDH) represents the small domain region of differences between the monomers. Red elliptical dashed line represents the extended C-terminal domain. (For interpretation of the references to color in this figure legend, the reader is referred to the web version of this article.)

3.2. Active site

The citrate molecule is located at the active site, and interacting with residues at the cleft between the large and small domains (Supplemental Fig. S2a and Fig. 2). The catalytic triad residues Lys191, Asp248 and Tyr144 are conserved and interacting with citrate (Supplemental Fig. S1). The citrate molecule (CIT) interacts with residues from two sub-unit interface, cofactor ($NADP^+$) and water molecules (W1 and W2). The C1 corboxyl hydrogen bonds to the ribose (of $NADP^+$) along with residues Thr90, Ser98 and

water molecule W2. Atom O7 (C3) hydrogen bonds to Lys191 and W2. The C5 hydrogen bonds to water molecule (W1), Arg137, Arg114 and Arg104. The C5 carboxyl establishes hydrogen bond network to Lys191 and Arg104. Further, water molecules W1 connects to Asp224 and Asp248 through hydrogen bonds. While, W2 hydrogen bonds to Asn193 and Asp224. The amide of nicotinamide ring moiety ($NADP^+$) interacts with the atom O2 of the citrate (Supplemental Fig. S2b and c). The bond distances are tabulated in Table 2

3.3. $NADP^+$ binding site

The atomic model of $NADP^+$ molecule was completely established with the available electron density (Supplemental Fig. S3a). The cofactor interacts with the residues of two subunits, citrate and water molecules. (Fig. 3A–C). The $NADP^+$ is divided into A2P (adenosine-2′, 5′-biphosphate) and NMN (nicotinamide mononucleotide) moieties over O3 atom (Supplemental Fig. s3b) [19]. The adenine ring and the endocyclic ribose (oxygen) adopt the typical *anti*-conformation with respect to each other around the N-glycosidic bond, and the ribose ring binds in an almost half-chair C2′-exo/C3′-endo conformation [19–20]. The N1A and N6A atoms of the adenine ring make direct hydrogen bonds with residues Asn293 (N, 3.27 Å) and Asn293 (O, 2.83 Å), respectively. The phosphate moiety (O3X) directly interacts with W4 (2.84 Å) and Tyr286 (OH, 2.70 Å). Also, interacts to the N3A (3.00 Å) of adenine ring through water molecule (W4). The residue Gln229 (NE2, 3.14 Å) and water molecule (W1, 2.91 Å) directly hydrogen bonds to the O2X. Also, Arg233 (NE – 2.64 Å, NH2 – 3.0 Å) connects to it through W1. The water molecule (W2, 3.11 Å) connects Asn225 (ND2, 3.12 Å) and Lys285 (NZ, 2.69 Å) to atom O1X. The O3X hydrogen bonds to Tyr286 (OH, 2.70 Å). The O3B of ribose moiety (A2P) connects to water molecule (W6, 2.82 Å) which acts as a bridge to O1N (2.87 Å) of pyrophosphate moiety (NMN). The residues Gly281 (N, 2.77 Å) and Ala282 (N, 3.00 Å) makes hydrogen bonds to O1A and O2A atoms, respectively. In the NMN moiety the nicotinamide ring adopts bent conformation. The ribosyl ring adopts half-chair C2'-exo/C3'-endo conformation making a dihedral angle of 158° about the O5D-C5D phosphoester bond. The amide moiety, N7N hydrogen bonds to O2 atom of the citrate with a distance 2.78 Å and to the residue Glu277 (OE1, 3.15 Å). The atom O7 forms a hydrogen bond to the Leu88 (N, 2.89 Å), while 3′-hydroxyl (O3D) forms a hydrogen bond with Thr90 (N, 2.64 Å). 2′-hydroxyl (O2D) interacts with Asn193 (ND2, 2.96 Å) and the 4′-hydroxyl (O4D) forms a hydrogen bond with Ser282 (N, 3.15 Å). The pyrophosphate moiety atom O2N hydrogen bonds to the water molecule (W5, 2.76 Å) and connected to Asp224 through water molecule W5 (OD1, 2.67 Å). Also, this moiety hydrogen bonds to the water molecule (W3, 2.69 Å). Further extending interaction from water molecule (W3) to Asn225 (ND2, 2.98 Å) and Ile222 (N, 3.01 Å).

Table 2
Hydrogen bonding distance between citrate, water molecules and the residues.

Citrate atom name	Interacting residue (atom name)	Distance in Å
O1	Arg114 (NH2)	2.90
	Arg137 (NH1)	3.09
	W2	2.69
O2	Arg104 (NH2)	2.59
	NADP+ (N7N)	2.78
O3	W1	2.95
O4	Thr90 (OG1)	2.76
	Ser98 (OG)	2.67
O5	Lys191 (NZ)	3.02
O6	Arg104 (NH1)	2.84
O7	W1	2.85
	Lys191 (NZ)	3.02
	W2	3.05
Water		
W1	Lys191 (NZ)	3.09
	Asp224 (OD2)	2.96
	Asn193 (ND2)	2.78
W2	Asp248 (OD1)	2.47
	Asp224 (OD2)	2.47

3.4. Oligomerization

*Tt*IDH exhibits a novel dimerization when compared to the earlier reported structures of *Bs*IDH, *Ap*IDH, and *Ec*IDH. The clasp region helices (Fig. 2: red arrow) is absent in the *Tt*IDH structure, where these helices are observed in the structures of *Bs*IDH, *Ap*IDH and *Ec*IDH. The absence of clasp region in *Tt*IDH is compensated by the novel C-terminal domain interacting through α14, β16 and β19 folds (Supplemental Fig. S4c). Therefore, unique dimerization is formed in *Tt*IDH through the novel terminal domain. The dimeric interface area of the *Tt*IDH (5610 $Å^2$) is large when compared to the other *Bs*IDH (3630 $Å^2$), *Ap*IDH (2950 $Å^2$), and *Ec*IDH (3300 $Å^2$). A surface area of 790 $Å^2$ is provided by C-terminal domain of *Tt*IDH (Supplemental Fig. S4a–c).

We observed 94 hydrogen bonds between the dimers, salt bridges (Supplemental table a), aromatic–aromatic (Tyr126, A-Tyr126, B, 5.90 Å) interaction and cation–pi interaction are observed (Supplemental table b). These interactions leading to oligomerization enhances the enzyme to perform at higher temperature [36].

3.5. Structural comparison

A 3-D structural similarity search using DALI [32] server was performed between *Tt*IDH and available structures in the Protein Data Bank (PDB). The search revealed several enzymes categorized under IDH family fold with *Z* scores of 45.1–41.2 and with r.m.s.d. values of 1.4–3.0 Å. The top most similar enzymes is NAD dependent *Acidithiobacillus thiooxidans* IDH (PDB: 2D4V, *Z*-score of 45.6, 39% sequence identity, r.m.s.d. 1.8 Å for 347 C_α atoms) [37], followed by type *Ec*IDH (PDB: 4AJ3, *Z*-score of 45.1, 39% sequence identity, r.m.s.d. 1.8 Å for 346 C_α atoms), *Ap*IDH (PDB: 1XKD, *Z*-score of 45.0, 38% sequence identity, r.m.s.d. 2.1 Å for 348 C_α atoms) and *Bs*IDH (PDB: 1HQS, *Z*-score of 44.7, 39% sequence identity, r.m.s.d. 1.9 Å for 347 C_α atoms). The two structures (*Tt*IDH and *Ec*IDH) are superposed (Fig. 4) and structural difference at the clasp domain and in the small domain were clearly identified. The clear overlapping of NADP loop and phosphorylation loop of both *Tt*IDH and *Ec*IDH suggests that they are "in" state. Therefore overall conformation of the *Tt*IDH may be closed.

3.6. Catalytic mechanism

Attempt was made to co-crystallize *Tt*IDH with the isocitrate and metal-ion, but failed to have ternary complex crystals. However, citrate binding at the active site provided the structural environment similar to the substrate binding. The chemical structures of citrate and isocitrate are isomers (Supplemental Fig. S6) and thus citrate may be regarded as a substrate. In order to understand the catalytic mechanism of the *Tt*IDH as proposed by Atkas and Cook [38] with the *Ec*IDH structural data [19], we made an attempt to induce by structural superposition of isocitrate (*Ec*IDH; PDB: 4aj3) into the active site pocket on the basis of binding of citrate (*Tt*IDH). The isocitrate and citrate binds to the same position (Supplemental Fig. S6) along with the metal ion (Ca^{2+}), making a modeled ternary complex. The hydride ion from C2 is transferred to C4N of the $NADP^+$ resulting NADPH [3,19,39].

The Lys191 (Lys230 of *Ec*IDH) forms a hydrogen bond with a distance of 3.3 Å (3.2 Å in *Ec*IDH) with the substrate C2 hydroxyl.

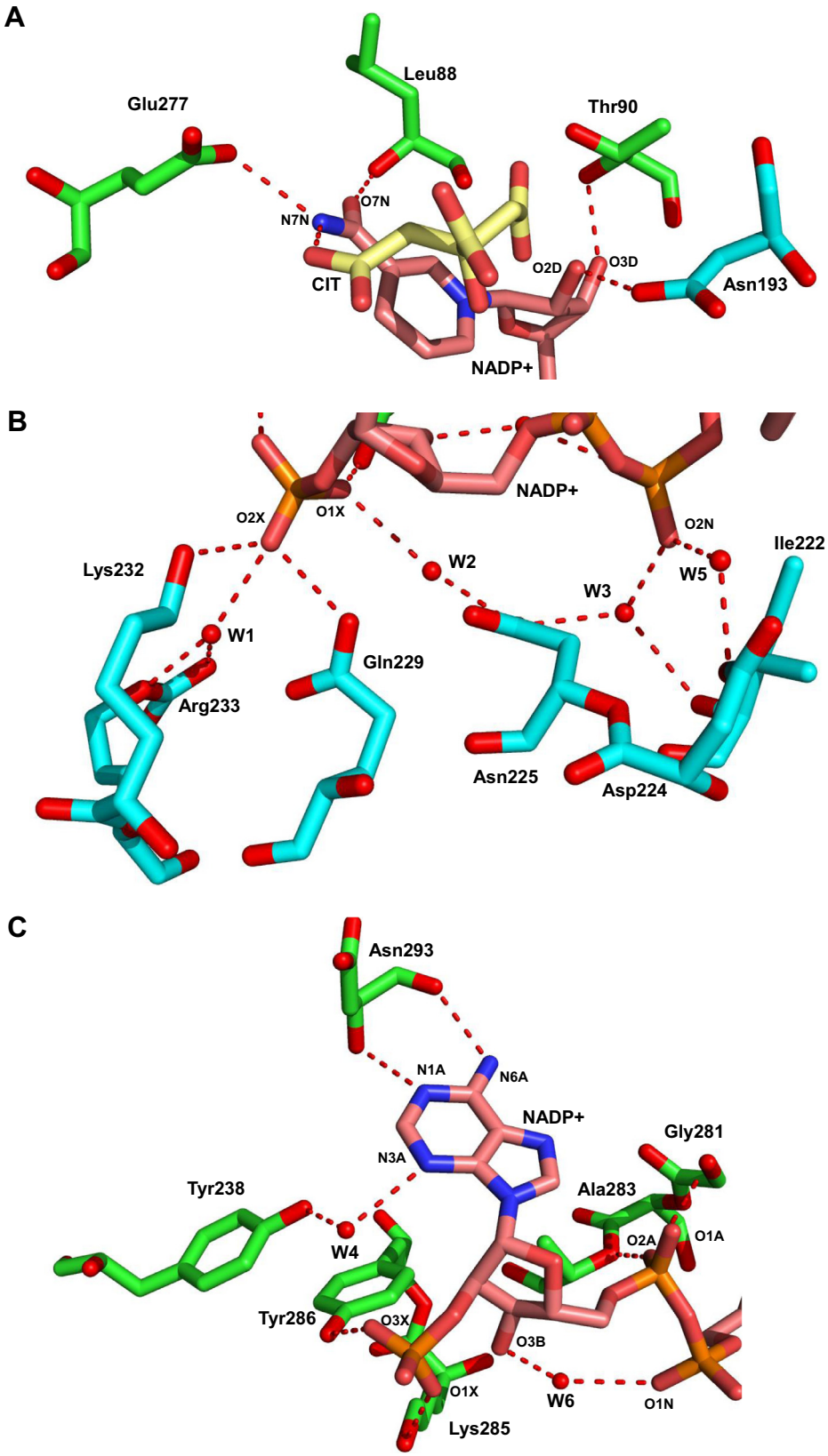

Fig. 3. The interaction of NADP+ (brown, stick model) and residues from the same monomer are represented by green color. The citrate (CIT) is represented by yellow colored stick model. The residues from the other subunit are represented by cyan stick model. Water molecules are represented by red sphere. (A) The nicotinamide part of NADP+ (brown stick model) interacting with residues Leu88, Thr90, Glu277 and Asn193. (B) The phosphate moiety interacting with residues Lys232, Arg233, Gln229, Asn225, Asp224, Ile222 and water molecules (W1, W2, W3, W5). (C) The adenosine and ribose moiety making interaction with residues Tyr238, Tyr286, Lys285, Ala283, Gly281, Asn293 and water molecules (W4, W6). (For interpretation of the references to color in this figure legend, the reader is referred to the web version of this article.)

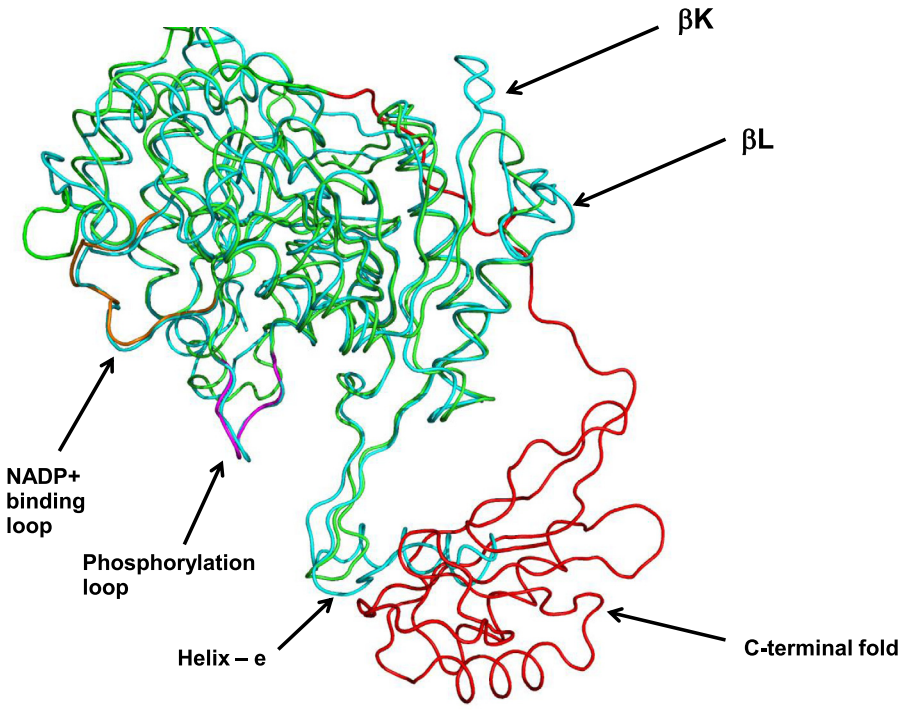

Fig. 4. Superimposition of *Tt*IDH (green ribbon) and *Ec*IDH (cyan ribbon) secondary structures. The extended C-terminal domain of *Tt*IDH is colored red. The arrows indicate βK and βL of *Ec*IDH which is not observed in *Tt*IDH. The dashed line indicates the absence of helix in clasp domain of *Tt*IDH, which is present in the *Ec*IDH (helix-e). The NADP binding loop is colored orange for *Tt*IDH and phosphorylation loop by magenta. These loops overlap well with NADP and phosphorylation loops of *Ec*IDH. (For interpretation of the references to color in this figure legend, the reader is referred to the web version of this article.)

The Asp248 adopt the same conformation as the corresponding Asp307 from *Ec*IDH and involved in decarboxylation. Here, Tyr144 (Tyr160 of *Ec*IDH) doesn't make any hydrogen bond with the isocitrate and results in the loss of its interaction with β -carboxylate group of isocitrate. This clearly indicates the need of metal ion for the completion of catalysis. According to the proposed catalytic mechanism [39], the Tyr144 should make hydrogen bond with the Lys191 to perform dehydrogenation and decorboxylation. The proton relay configured with O2N (of $NADP^+$) and water molecules (W3, W5 and W7) (Supplemental Fig. S6) are observed as reported [19,21]. In conclusion, *Tt*IDH performs similar catalytic mechanism as proposed using structural data *Ec*IDH [19].

In this study, we have determined the three-dimensional structure of $NADP^+$ dependent ternary complex *Tt*IDH structure (citrate and $NADP^+$ molecule) using X-ray diffraction method. We observed the monomeric structure consists of a unique, novel C-terminal domain, which is involved in the oligomerization. The overall interface area between the dimers is large when compared to the other reported IDH's. The cofactor $NADP^+$ and citrate molecule was bound at the cleft between the two adjacent subunits. The crystal structure of homodimeric $NADP^+$ dependent *Tt*IDH with a novel C-terminal domain may provide evidence in framing an additional subfamily of the type IV.

Acknowledgments

Authors would like to thank the staff of RIKEN Genomic Sciences Center for providing the plasmid, and the beamline staff for assistance during data collection at beamline BL26B1 of SPring-8, Japan. The authors would like thank the IOE X-ray diffraction facility, University of Mysore, Mysore, for collecting the data. One of the authors, S. Madan Kumar thanks UGC-BRS for providing RFSMS fellowship.

Appendix A. Supplementary data

Supplementary data associated with this article can be found, in the online version, at http://dx.doi.org/10.1016/j.bbrc.2014.04.164.

References

[1] L. Stryer, Biochemistry, W. H. Freeman and Company, New York, 1988. p. 375.
[2] A.M. Dean, G.B. Golding, Protein engineering reveals ancient adaptive replacements in isocitrate dehydrogenase, Proc. Natl. Acad. Sci. U.S.A. 94 (1997) 3104–3109.
[3] X. Xu, J. Zhao, Z. Xu, B. Peng, Q. Haung, E. Arnold, J. Ding, Structures of human cytosolic NADP-dependent isocitrate dehydrogenase reveal a novel self-regulatory mechanism of activity, J. Biol. Chem. 279 (2004) 33946–33957.
[4] G. Zhu, G.B. Golding, A.M. Dean, The selective cause of an ancient adaptation, Science 307 (2005) 1279–1282.
[5] R. Chen, S.S. Jeong, Functional prediction: identification of protein orthologs and paralogs, Protein Sci. 9 (2000) 2344–2353.
[6] M. Karlstrom, I.H. Steen, D. Madern, A.E. Fedoy, N.K. Birkland, P. Landenstein, The crystal structure of a hyperthermostable subfamily II isocitrate dehydrogenase from *Thermotoga maritime*, FEBS J. 273 (2006) 2851–2868.
[7] D.C. LaPorte, T. Chung, A single gene codes for the kinase and phosphate which regulate isocitrate dehydrogenase, J. Biol. Chem. 260 (1985) 15291–15297.
[8] M. Garnak, H.C. Reeves, Phosphorylation of isocitrate dehydrogenase of *Escherichia coli*, Science 203 (1979) 1111–1112.
[9] D.C. LaPorte Jr., D.E. Koshland, A protein with kinase and phosphotase activities involved in the regulation of tricarboxylic acid cycle, Nature 300 (1982) 459–460.
[10] J. Zheng, Z. Jia, Structure of the bifunctional isocitrate dehydrogenase kinase/phosphatase, Nature 465 (2010) 961–965.
[11] B. Yang, C. Zhong, Y. Peng, Z. Lai, J. Ding, Molecular mechanisms of "off–on switch" of activities of human IDH1 by tumor-associated mutation R132H, Cell Res. 20 (2010) 1188–1200.
[12] B. Zheng, Y. Yao, Z. Liu, L. Deng, J.L. Anglin, H. Jiang, B.V. Prasad, Y. Song, Crystallographic investigation and selective inhibition of mutant isocitrate dehydrogenase, Med. Chem. Lett. 4 (2013) 542–546.
[13] C.E. Quartararo, S. Hazra, T. Hadi, J.S. Blanchard, Structural, kinetic and chemical mechanism of isocitrate dehydrogenase-1 from *Mycobacterium tuberculosis*, Biochemistry 52 (10) (2013) 1765–1775.
[14] S. Kim, S.Y. Kim, H.J. Ku, Y.H. Jeon, H.W. Lee, J. Lee, T.K. Kwon, K.M. Park, J.W. Park, Suppression of tumorigensis in mitochondrial NADP+-dependent

isocitrate dehydrogenase knock-out mice, Biochim. Biophys. Acta (BBA)-Mol. Basis Dis. 1842 (2014) 135–143.
[15] M.M. Jin, P. Wang, X. Li, X.Y. Zhao, L. Xu, P. Song, G.P. Zhu, Biochemical characterization of NADP+-dependent isocitrate dehydrogenase from *Microcystis aeruginosa* PCC7806, Mol. Biol. Rep. 40 (2013) 2995–3002.
[16] I.H. Steen, D. Madren, M. Karlstorm, T. Lein, P. Landenstein, N.K. Birkland, Comparison of isocitrate dehydrogenase from three hyperthermophiles reveals differences in thermostability, cofactor specificity, oligomeric state and phylogenetic affiliation, J. Biol. Chem. 276 (2001) 43924–43931.
[17] R. Vinekar, C. Verma, I. Ghosh, Functional relevance of dynamic properties of dimeric NADP-dependent isocitrate dehydrogenases, BMC Bioinformatics 13 (Suppl. 17) (2012) S2.
[18] J.H. Hurley, A.M. Dean Jr., D.E. Koshland, R.M. Stroud, Catalytic mechanism of NADP(+)-dependent isocitrate dehydrogenase: implications from the structures of magnesium-isocitrate and NADP+ complexes, Biochemistry 30 (1991) 8671–8678.
[19] S. Goncalves, P.S. Miller, M.A. Carrondo, A.M. Dean, P.M. Matias, Induced fit and the catalytic mechanism of isocitrate dehydrogenase, Biochemistry 51 (2012) 7098–7115.
[20] S.K. Singh, K. Matsuno, D.C. LaPorte, L.J. Banaszak, Crystal structure of *Bacillus subtilis* isocitrate dehydrogenase at 1.55 Å. Insights into the nature of substrate specificity exhibited by *Escherichia coli* isocitrate dehydrogenase kinase/phosphatase, J. Biol. Chem. 276 (2001) 26154–26163.
[21] M. Karlstrom, R. Stokke, I.H. Steen, N.K. Birkland, R.P. Ladensteinet, Isocitrate dehydrogenase from the hyper-thermophile *Aeropyrum pernix*: X-ray structure analysis of a ternary enzyme-substrate complex and thermal stability, J. Mol. Biol. 345 (2005) 559–577.
[22] W.A. Hendrickson, J.R. Horton, D.M. LeMaster, Selenomethionyl proteins produced for analysis by multiwavelength anomalous diffraction (MAD): a vehicle for direct determination of three-dimensional structure, EMBO 9 (1990) 1665–1672.
[23] Z. Otwinowski, W. Minor, Processing of X-ray diffraction data collected in oscillation mode, Meth. Enzymol. 276 (1997) 307–326.
[24] Collaborative Computational Project, Number 4, The CCP4 suite: programs for protein crystallography, Acta Crystallogr. D: Biol. Crystallogr. 50 (1994) 760–763.
[25] T.C. Terwilliger, J. Berendzen, Automated MAD and MIR structure solution, Acta Crystallogr. D: Biol. Crystallogr. 55 (1999) 849–861.
[26] A.T. Brunger, P.D. Adams, G.M. Clore, W.L. DeLano, P. Gross, R.W. Grosse-Kunstleve, J.S. Jiang, J. Kuszewski, M. Nilges, N.S. Pannu, L.M. Rice, T. Simson, G.L. Warren, Crystallography & NMR System: a new software suite for macromolecular structure determination, Acta Crystallogr. D: Biol. Crystallogr. 54 (1998) 905–921.
[27] G.J. Kleywegt, T.A. Jones, Acta Crystallogr. D: Biol. Crystallogr. 54 (1998) 1119–1131.
[28] R.A. Laskowski, M.W. MacArthur, D.S. Moss, J.M. Thornton, PROCHECK: a program to check the stereochemical quality of protein structures, J. Appl. Cryst. 26 (1993) 283–291.
[29] L. Holm, C. Sander, Dali: a network tool for protein structure comaprision, Trends Biochem. Sci. 20 (1995) 478–480.
[30] E. Krissinel, K. Henrick, Detection of protein assemblies in crystals, in: Berhold Mrea (Ed.), Computational Life Sciences, Springer, Heidelberg Berlin, 2005, pp. 163–174.
[31] (a) S. Kumar, R. Nussinov, Salt bridge stability in monomeric proteins, J. Mol. Biol. 293 (1999) 1241–1255;
(b) S. Kumar, C.J. Tsai, B. Ma, R. Nussinov, Contribution of salt bridges toward protein thermostability, J. Biomol. Struct. Dyn. 1 (2000) 79–85;
(c) S. Kumar, R. Nussinov, Relationship between ion pair geometries and electrostatic strengths in proteins, Biophys. J. 83 (2002) 15595–15612;
(d) J.N. Sarakatsannis, Y. Duan, Statistical characterization of salt bridges in proteins, Proteins 60 (2005) 732–739.
[32] K.G. Tina, R. Bhadra, R. Srinivasan, PIC: protein interactions calculator, Nucleic Acids Res. 35 (2007) W473–W476.
[33] J.D. Thompson, D.G. Higgins, T.J. Gibson, CLUSTAL W: improving the sensitivity of progressive multiple sequence alignment through sequence weighting, position-specific gap penalties and weight matrix choice, Nucleic Acids Res. 22 (1994) 4673–4680.
[34] P. Gouet, E. Courcelle, D.I. Stuart, ESPript: analysis of multiple sequence alignments in PostScript, Bioinformatics 15 (1999) 305–308.
[35] B.W. Mathhews, Solvent content of protein crystals, J. Mol. Biol. 33 (1968) 491–497.
[36] N.K. Lokanath, I. Shiromizu, N. Ohshima, Y. Nodakke, M. Sugahara, S. Kuramitsu, M. Miyano, N. Kunishima, Structure of aldolase from *Thermus thermophilus* HB8 showing the contribution of oligomeric state to thermostability, Acta Cryst. D60 (2004) 1816–1823.
[37] K. Imada, T. Tamura, R. Takenaka, I. Kobayashi, K. Namba, K. Inagaki, Structure and quantum chemical analysis of NAD+-dependent isocitrate dehydrogenase: hydride transfer and co-factor specificity, Proteins: Struct. Funct. Bioinformatics 70 (2007) 63–71.
[38] D.F. Aktas, P.F. Cook, A lysine-tyrosine pair carries out acid-base chemistry in the metal ion-dependent pyridine dinucleotide-linked beta-hydroxyacid oxidative decarboxylases, Biochemistry 48 (2009) 3565–3577.